Indian J Phys
DOI 10.1007/s12648-016-0909-7

ORIGINAL PAPER

Ab initio study of the electronic, optical and thermodynamic properties of the ternary phosphides Li*Ae*P (*Ae* = Sr, Ba)

A Benahmed[1], A Bouhemadou[1]*, R Khenata[2] and S Bin-Omran[3]

[1]Laboratory for Developing New Materials and Their Characterization, University of Setif 1, 19000 Sétif, Algeria

[2]Laboratoire de Physique Quantique de la Matière et de Modélisation Mathématique (LPQ3M), Université de Mascara, 29000 Mascara, Algeria

[3]Department of Physics and Astronomy, College of Science, King Saud University, P.O. Box 2455, Riyadh 11451, Saudi Arabia

Received: 25 December 2015 / Accepted: 05 July 2016

Abstract: We report the results of an ab initio study of the electronic, optical and thermodynamic properties of the LiBaP and LiSrP compounds using the pseudopotential plane-wave method within the framework of the density functional theory with the GGA-PBEsol. The calculated equilibrium structural parameters are in good agreement with the available experimental data. The energy band dispersions along the high symmetry directions in the *k*-space and the density of states diagrams are computed and analyzed. The obtained energy bands show that both examined crystals are indirect band gap semiconductors. The chemical bonding character is examined via electron density map plots. The optical properties are predicted for an incident radiation in an energy range up to 15 eV, and the origins of the main peaks in the optical spectra are discussed in terms of the calculated electronic band structure. We have also predicted the temperature and pressure dependencies of the unit-cell volume, thermal expansion coefficient, heat capacity, Debye temperature and Grüneisen parameter.

Keywords: Ternary phosphides; Ab initio calculations; Electronic structure; Optical properties; Thermal effect

PACS Nos.: 71.15.Mb; 71.20.Nr; 78.20.-e; 71.20.-b; 65.40.-b

1. Introduction

Ternary compounds with a simple 1:1:1 composition—so-called 111 phase —crystallize in more than 30 structure types [1]. In recent years, these ternary compounds, especially the half Heusler structure (archetype MgAgAs), the LiGaGe structure, the ZrBeSi structure and the TiNiSi structure, have drawn increasing attention due to their interesting physical properties, which make them candidates for many technological applications. For example, the half Heusler compounds are known to be good thermoelectrics [2–4] and have been proposed as topological insulators [5, 6]. The LiGaGe structure type systems have been proposed as ferroelectrics [7]. The ZrBeSi type compounds have been proposed as Dirac semimetals [8]; three-dimensional (3D) topological Dirac semimetals (TDSs) are a recently proposed state of quantum matter [9–14] that has attracted increasing attention in physics and materials science. Generally, the 111 phases are semiconductor materials. The interest in the ternary semiconductor 111 phases is due to the attractive chemistry encountered in this class of inorganic compounds and to their excellent physical properties that are not possessed by the simple and binary semiconductors owing to the presence of three different chemical elements [15].

Recently, Dong et al. [16] synthesized several ternary phosphide single crystals, including the LiSrP and LiBaP systems. The considered LiSrP and LiBaP compounds are initially discovered in syntheses designed to explore the existence of a new class of materials containing both nitrogen and phosphorus as anions. Their crystalline structures are determined using the single-crystal X-ray diffraction. Both compounds adopt a centrosymmetric hexagonal structure, space group $P6_3/mmc$ (ZrBeSi structure), with two formula units by unit-cell (Z = 2) [17]. Apart from the experimental results regarding the synthesis and structural parameters reported by Dong and co-authors

*Corresponding author, E-mail: a_bouhemadou@yahoo.fr

Published online: 23 August 2016

[16], no theoretical or experimental data are available in the scientific literature for the considered systems to the best of our knowledge. Therefore, from a fundamental standpoint and in terms of eventual technological applications, we have performed the present work to obtain some of the lacking data.

Ab initio methods based on the density functional theory (DFT) have become a very powerful tool for exploring the properties of materials without requiring any experimental measurement. Thus, ab initio calculations using the pseudopotential plane-wave in the DFT framework have been performed to investigate the electronic, optical and thermodynamic properties of the Li*Ae*P (*Ae* = Sr and Ba) compounds.

2. Calculation details

All calculations were carried out using the pseudopotential plane-wave method based on the DFT, as implemented in the CASTEP (Cambridge Serial Total Energy Package) code [18]. The exchange–correlation potential was modeled using the generalized gradient approximation of Perdew et al. (so-called GGA-PBEsol) [19]. The interactions between the valence electrons and the ion cores were described by means of the Vanderbilt ultrasoft pseudopotentials [20]. The Li: $1s^2 2s^1$, P: $3s^2 3p^3$, Ba: $4d^{10} 5s^2 5p^6 6s^2$ *and* Sr: $3d^{10} 4s^2 4p^6 5s^2$ states were treated as valence electrons. The cut-off energy, which determines the size of the plane-wave basis set, was 400 eV. The integration over the Brillouin zone (BZ) was carried out using the Monkhorst–Pack sampling method [21] with a 9 × 9×6*k*-points grid. The self-consistent field was considered to be converged when the change in total energy was less than 1×10^{-6} eV/atom. The structural optimizations were performed using the Broyden–Fletcher–Goldfarb–Shanno (BFGS) minimization scheme [22]. The tolerances were set as the difference in total energy within 5×10^{-6} eV/atom, the maximum ionic Hellmann–Feynman force within 0.01 eV/Å, the maximum ionic displacement within 5×10^{-4} Å and the maximum stress within 0.02 GPa.

3. Results and discussion

3.1. Structural parameters

The examined LiSrP and LiBaP systems crystallize in a hexagonal crystal structure, space group $P6_3/mmc$ (no. 194), with two formula units per unit-cell. The Wyckoff positions of atoms are as follows: Li: 2*c* (1/3, 2/3, 1/4), Sr, Ba: 2*a* (0, 0, 0) and P: 2*d* (1/3, 2/3, 3/4) [16]. The calculated equilibrium lattice parameters, a_0 and c_0, for LiSrP and LiBaP are tabulated in Table 1, together with the available experimental data for comparison. One can appreciate that the relative deviations of the calculated equilibrium lattice parameters a_0 and c_0 from the measured ones do not exceed 0.26 and 0.96 %, respectively, in LiSrP and 0.12 and 0.65 %, respectively, in LiBaP. This good consistency proves the reliability of the calculation method. The lattice parameters (a_0 and c_0) of LiBaP are larger than those of LiSrP. This trend can be explained by considering the atomic radii of Ba and Sr atoms as follows: $R(Ba) = 215pm > R(Sr) = 200pm$.

3.2. Electronic band structure and chemical bonding

Investigation of the electronic energy bands of the LiBaP and LiSrP ternary compounds would be very useful to better understand their electronic and optical properties. The electronic energy band dispersions along the high symmetry lines in the first Brillouin zone of both examined crystals are depicted in Fig. 1. The topmost of the valence bands (VB) is located at the Γ-point in the Brillouin zone and the bottommost of the conduction bands (CB) is positioned at the M-point. Hence, both investigated systems are indirect band gap (Γ–M) semiconductors. The fundamental band gap of LiSrP (LiBaP) is equal to 1.16 eV (0.80 eV). No experimental or theoretical data are available in the scientific literature for the band gaps of LiSrP and LiBaP for comparison with our findings. Bearing in mind that the DFT within the common GGA underestimates the band gaps of semiconductors and isolators, the predicted values in the present work can serve as minimum estimates of the true band gaps of the considered crystals. The band gap calculated using the DFT with the common GGA is likely to be approximately 30−50 % smaller than the experimental values [23]. Therefore, the real fundamental band gap of LiSrP (LiBaP) is expected to be in the range 1.50–1.73 eV (1.04–1.20 eV). The replacement of Sr with Ba in the Li*Ae*P series (*Ae*: Sr, Ba) leads to the narrowing of the band gap by approximately 31 %.

Table 1 Calculated equilibrium lattice parameters (a_0 and c_0, in Å), equilibrium unit-cell volume (V_0, in Å^3)

	a_0	c_0	c_0/a_0	V_0
LiSrP				
Present work	4.3557	7.9031	1.81	129.85
Expt. [3]	4.3674	7.9802	1.83	131.82
LiBaP				
Present work	4.4945	8.5483	1.90	149.54
Expt. [3]	4.5003	8.6049	1.91	150.92

Available experimental results are reported for comparison

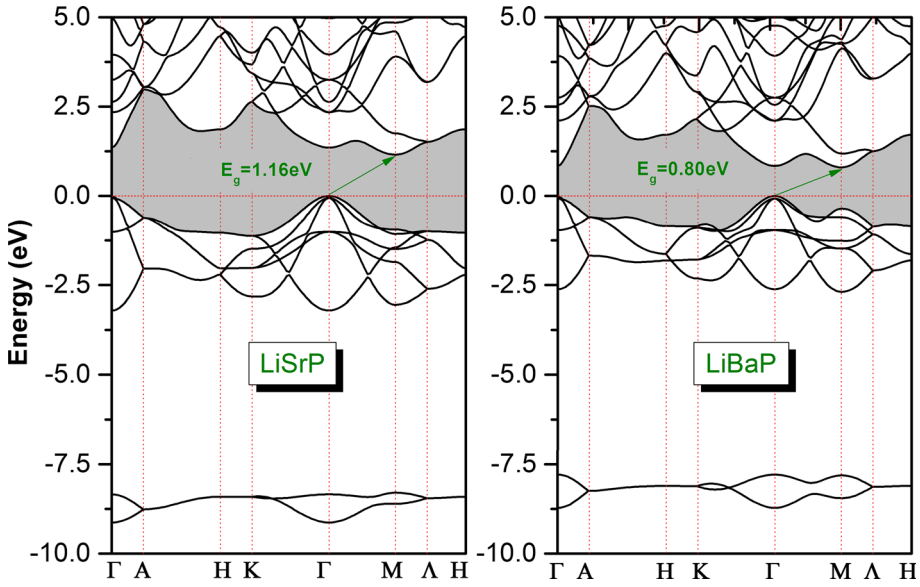

Fig. 1 Calculated electronic energy band dispersion curves along the high symmetry directions in the Brillouin zone for the Li*Ae*P (*Ae* = Sr, Ba) compounds. E_g gives the value of the fundamental energy band gap Γ–M. The Fermi level is given at 0.0 eV

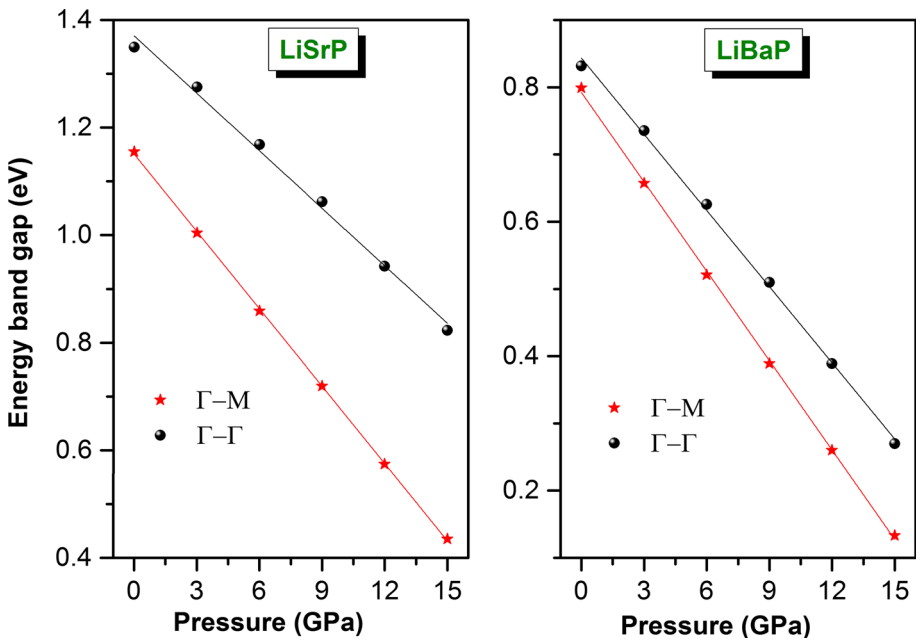

Fig. 2 Pressure dependence of the fundamental indirect band gap Γ-M and the first direct band gap Γ–Γ for the Li*Ae*P (*Ae* = Ba, Sr) compounds. The calculated values are indicated by *symbols* and the fits by *solid lines*

Figure 2 shows the pressure dependencies of the fundamental band gap Γ–M ($E_g^{\Gamma-M}(P)$) and the first direct band gap Γ−Γ ($E_g^{\Gamma-\Gamma}(P)$) of LiSrP and LiBaP in a pressure range between 0 and 15 GPa. First, the fundamental band gap remains between the topmost of the valence bands at the Γ-point and the bottommost of the conduction bands at the M-point for both examined compounds in the considered pressure range. Second, both considered gaps, i.e., Γ-M and Γ−Γ, are characterized by a quadratic decrease with increasing pressure in both compounds; the CB bottommost moves down with increasing pressure. When the pressure increases from 0 to 15 GPa, the fundamental band gap Γ-M decreases from 1.16 to 0.44 eV in LiSrP and from 0.80 eV to 0.13 eV in LiBaP. The first direct band gap, Γ−Γ, decreases from 1.35 to 0.82 eV in LiSrP and from 0.83 to 0.27 eV in LiBaP.

Knowledge of the effective mass values of the charge-carriers is necessary to determine the transport properties and electrical conductivity of materials; the conductivity is inversely proportional to the effective mass. In general, the theoretical effective mass is a tensor with nine components. However, for the very idealized simple case in which the energy $E(k)$ data are represented by a parabola curve, such as at the valence band maximum (VBMa) and the conduction band minimum (CBMi), the effective mass becomes a scalar that can be evaluated from the $E(k)$ curve

around the VBMa and CBMi by fitting the $E(k)$ data to the following well-known equation: $E = \frac{\hbar k^2}{2m^*}$, where ħ is Planck's constant, E is the band-edge energy as a function of the wave vector k and m^* is the effective mass. The calculated effective masses of the holes at the VBMa along the Γ-K and Γ−M directions and those of the electrons at the CBMi along the M−Γ and M−Γ directions are tabulated in Table 2. The results indicate that the electron effective mass has a relevant dependence on the k direction in both compounds, indicating its anisotropy, while the hole effective mass is quite isotropic. In addition, the hole effective mass value is close to that of the electron, suggesting that their mobilities will be fairly similar.

The total and atomic-resolved l-projected densities of states (TDOS and PDOS) corresponding to the energy bands of the LiSrP and LiBaP compounds are calculated to obtain information regarding the orbital character of the electronic states and the chemical bonding. The obtained DOS diagrams are depicted in Fig. 3. For the LiSrP compound, the lowest valence band group, located between approximately −10.0 and −8.0 eV, is essentially dominated by the P-3*s* orbitals with a small contribution from the Li-1*s*, Sr-4*s* and Sr-3*d* states. The lower part of the valence band group, ranging from −3.13 eV up to the Fermi level, consists mainly of the Sr-3*d*4*p* and P-3*p* states, whereas the upper part is due to the hybridized *Li*-1s, Sr-3*d* and P-3*p* states. The conduction bands ranging from 0 to 10 eV are composed principally of the Li-2*s*, Sr-3*d* and Sr-5*s* states, with a minor contribution from the P-3*s* states. For the LiBaP compound, the lowest valence band group, located between approximately −10.0 and −7.4 eV, is essentially dominated by the P-3*s* orbitals, with a small presence of the Ba-5*s* and Ba-4*d* states. The lower part of the upper valence band group, ranging from −2.98 eV up to the Fermi level, is formed mainly from the Ba-4*d*5*p* and P-3*p* states, whereas the upper part is due to the hybridized Li-1s, Ba-*d* and P-3*p* states. The conduction bands ranging from 0 to 10 eV are composed primarily of the Ba-4*d* and Li-2*s* states with a small contribution from the Ba-6*s* and P-3*p* states.

To visualize the character of the chemical bonding between the constituent atoms, the valence charge density distribution maps of the investigated systems in the (110) plane are plotted in Fig. 4. The figure shows that a certain accumulation of electrons occurs between the P and Sr/Ba and between the P and Li atoms, indicating that the chemical bonding between those atoms is mostly covalent. The covalent bonding between P and Sr/Ba is due to the hybridization between the P-3*p* and Sr-3*d*/*Ba*-4d states, and the covalent bonding between P and Li is due to the hybridization between the P-3*p* and Li-2 *s* states.

Table 2 Calculated electron and hole effective masses (m_e^* and m_h^*, respectively; in units of free electron mass) for the LiSrP and LiBaP compounds

System	$m_e^*(\mathrm{M}-\Gamma)$	$m_e^*(\mathrm{M}-\Lambda)$	$m_h^*(\Gamma-\mathrm{K})$	$m_h^*(\Gamma-\mathrm{M})$
LiSrP	0.0668	0.0492	0.0437	0.0438
LiBaP	0.0579	0.0390	0.0337	0.0337

3.3. Optical properties

In the linear response range, the macroscopic optical response functions of solids can usually be described by the frequency-dependent dielectric function $\varepsilon(\omega) = \varepsilon_1(\omega) + i\varepsilon_2(\omega)$ or by the frequency-dependent complex refractive index $\tilde{n}(\omega) = n(\omega) + ik(\omega)$ [24], which are related mainly to the electronic structures. The optical functions reflect the fine structure of the electron energy dispersions in the valence and conduction bands. It is well-known that the imaginary part, i.e., $\varepsilon_2(\omega)$, of the dielectric function $\varepsilon(\omega)$ constructs the bridge between the electronic structure and the interband transitions. The imaginary part $\varepsilon_2(\omega)$ can be calculated from the momentum matrix elements between the occupied and unoccupied wave functions with respect to the selection rules [25]. The real part $\varepsilon_1(\omega)$ can be calculated from the imaginary part $\varepsilon_2(\omega)$ via the Kramer–Kronig relationship [26]. Knowledge of the imaginary ($\varepsilon_2(\omega)$) and real ($\varepsilon_1(\omega)$) parts of the dielectric function allows one to calculate all the important optical characteristics of materials, such as the refractive index $n(\omega)$, optical reflectivity $R(\omega)$, extinction coefficient $k(\omega)$, absorption coefficient $\alpha(\omega)$ and energy-loss function $L(\omega)$, using the well-known relationships [27, 28]. Calculations of the optical properties require more k-points than ordinary self-consistent field calculations; a 20 × 20 × 20 k-points grid is used in the present work. The LiSrP and LiBaP compounds have a hexagonal structure and are thus optically biaxial systems. For this reason, the optical functions of the considered crystals are calculated for polarized incident radiation with electric field vector $\vec{E}$ parallel to the principal crystallographic axes, i.e., $\vec{E}//a$ ($\vec{E}//[100]$) and $\vec{E}//c$($\vec{E}//[001]$). Because some of the synthetized samples are polycrystalline, the optical spectra are also predicted for the polycrystalline phase.

The absorptive $\varepsilon_2(\omega)$ and dispersive $\varepsilon_1(\omega)$ parts of the dielectric function for both LiSrP and LiBaP are shown in Fig. 5. The figure displays noticeable differences between the magnitudes, shapes and locations of the main features and peaks in the $\varepsilon_2(\omega)/\varepsilon_1(\omega)$ spectra corresponding to $\vec{E}//a$ and $\vec{E}//c$, demonstrating a strong anisotropy of the dielectric response of these materials to the incident radiation. The absorption edge is slightly shifted toward lower energies for the $\vec{E}//c$ polarization in both compounds; the absorption edge starts at 1.003 eV (0.510 eV) for $\vec{E}//a$ and at 0.960 eV (0.4680 eV) for $\vec{E}//c$ in LiSrP (LiBaP). Now,

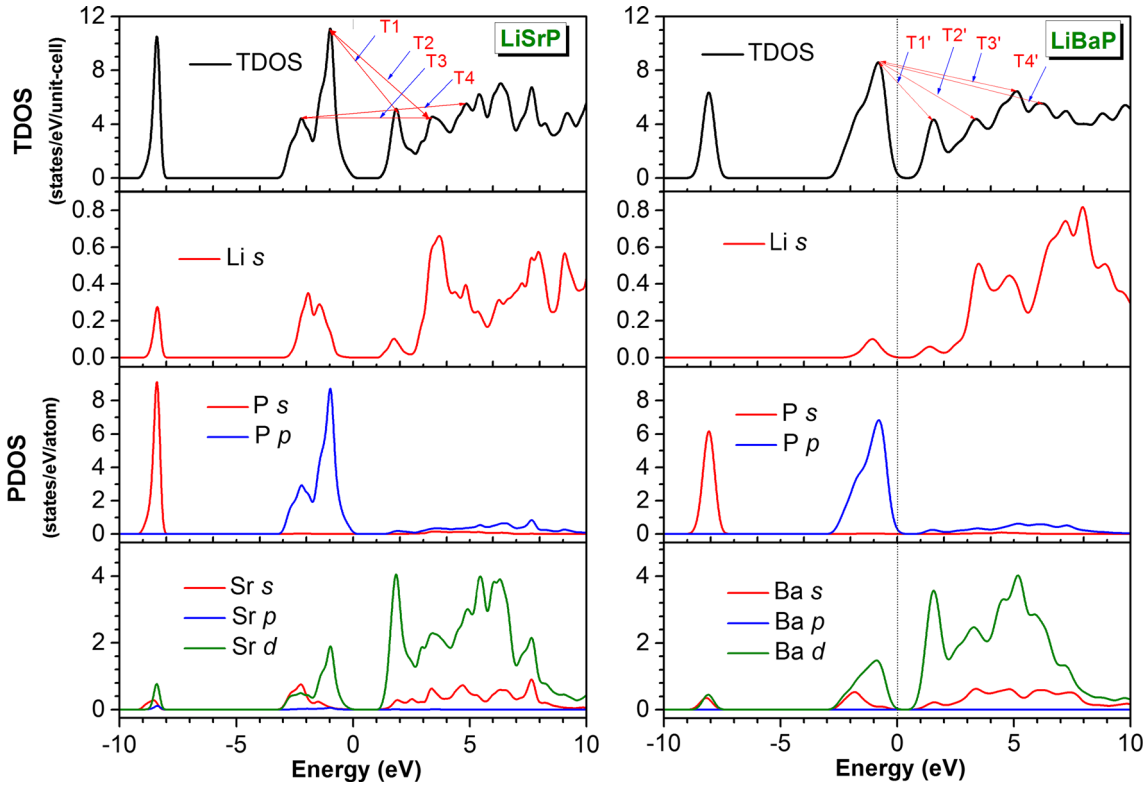

Fig. 3 Total (TDOS) and partial (PDOS) densities of states diagrams for the Li*Ae*P (*Ae* = Sr, Ba) compounds. T1 (T1′), T2 (T2′), T3 (T3′) and T4 (T4′) represent the electronic transitions from the valence bands to the conduction bands

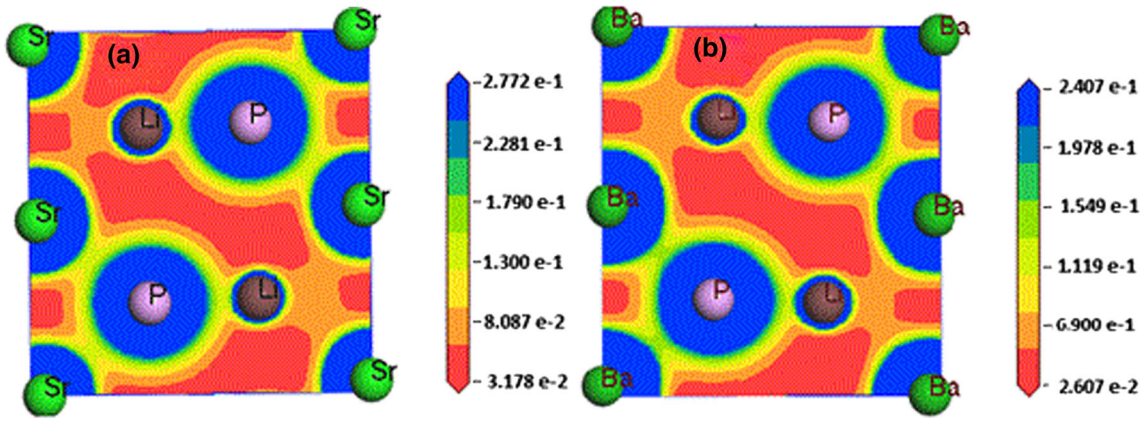

Fig. 4 Charge density distribution maps in the (110) plane for the LiSrP (**a**) and LiSrP (**b**) systems

we try to determine the origin of the occupied and unoccupied states involved in the direct interband transitions that caused the main peaks in the $\varepsilon_2(\omega)$ spectra based on the calculated electronic structure discussed in Sect. 3.2. The absorptive part $\varepsilon_2(\omega)$ of the dielectric function $\varepsilon(\omega)$ of LiSrP exhibits four structures labeled A, B, C and D. The lowest energy peak, A, centered at approximately 2.77 eV for $\vec{E}//a$ and 2.72 eV for $\vec{E}//c$, is caused by the interband transition T1 (see Fig. 3), which is due mostly to the electronic transitions from the Sr-3*d* and P-3*p* valence states to the Sr-3*d* conduction states. Structure B, centered at approximately 4.37 eV for $\vec{E}//a$ and 4.19 eV for $\vec{E}//c$, is due to the direct interband transition T2. Peak C, centered at approximately 5.23 eV for $\vec{E}//a$ and 6.68 eV for $\vec{E}//c$, is attributable to the direct interband transition T3, which is due mostly to the electronic transitions from the Sr-3*d*, P-3*p* and Li-2*s* valence states to the Sr-3*d* and Li-2*s* conduction states. The fourth peak, D, centered at approximately 5.66 eV for $\vec{E}//a$ and absent for $\vec{E}//c$, is caused by the direct interband transition T4. The $\varepsilon_2(\omega)$

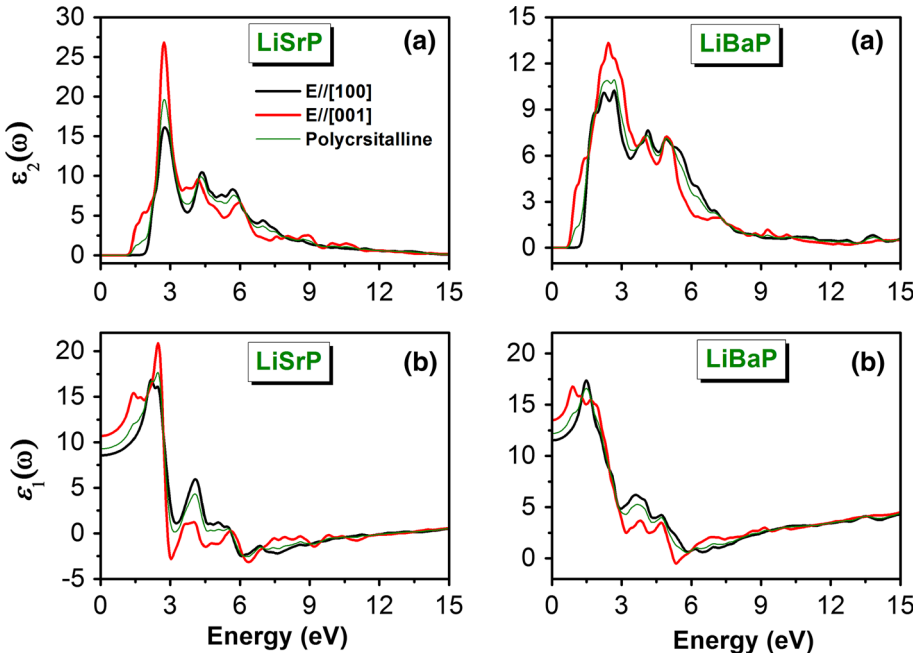

Fig. 5 Calculated (**a**) imaginary ($\varepsilon_2(\omega)$) and (**b**) real ($\varepsilon_1(\omega)$) parts of the dielectric function for incident radiation polarized along the two principal crystallographic directions, i.e., $\vec{E}//a$ and $\vec{E}//c$, for the Li*Ae*P (*Ae* = Sr, Ba) crystals. The obtained spectra for the Li*Ae*P (*Ae* = Sr, Ba) polycrystals are also shown

spectrum of LiBaP also exhibits four structures labeled A′, B′, C′ and D′. Peak A′, centered at approximately 2.23 eV for $\vec{E}//a$ and 2.67 eV for $\vec{E}//c$, is caused by the direct interband transition T1' (see Fig. 3) (mostly Ba-4*d* and P-3*p* → Ba-4*d*). Peak B′, centered at approximately 4.13 eV for $\vec{E}//a$ and 3.97 eV for $\vec{E}//c$, is due to the direct interband transition T2′. Peak C′, centered at approximately 4.92 eV for $\vec{E}//a$ and 4.93 eV for $\vec{E}//c$, is attributable to the direct interband transition T3′ (mostly Ba-4*d*, P-3*p* and Li-2 *s* → Ba-4*d* and Li-2*s*). The fourth peak, D′, centered at approximately 9.28 eV for $\vec{E}//a$ and absent for $\vec{E}//c$, is caused by the direct interband transition T4′. The zero frequency limit $\varepsilon_1(0) = \varepsilon_1(\omega \to 0)$—the electronic part of the static dielectric constant—is the most important quantity in the $\varepsilon_1(\omega)$ spectrum. The calculated value of $\varepsilon_1(0)$ for LiSrP (LiBaP) is equal to 8.569 (11.530) for $\vec{E}//a$ and 10.694 (13.498) for $\vec{E}//c$. The values of $\varepsilon_1(0)$ for both considered light polarizations in LiSrP are larger than their corresponding ones in LiBaP; i.e., $\varepsilon_1(0)$ increases with decreasing band gap. This trend can be explained on the basis of the Penn model [29]: $\varepsilon(0) \approx 1 + (\hbar\omega_p/E_g)^2$.

The absorption coefficient $\alpha(\omega)$ is a basic way to measure how far light with a specific energy can penetrate a material before being absorbed. The calculated absorption coefficients for LiSrP and LiBaP for both considered light polarizations, i.e., $\vec{E}//a$ and $\vec{E}//c$, are displayed in Fig. 6(a), in which the fundamental absorption edge starts approximately at 1.003 eV (0.510 eV) for $\vec{E}//a$ and 0.960 eV (0.468 eV) for $\vec{E}//c$ in LiSrP (LiBaP). The absorption coefficient increases with increasing photon energy, reaching a maximum and then decreasing to reach its minimum. The absorption spectrum shows some peaks that can be explained by the interband transitions using the band structure results. LiSrP has an absorptive energy region larger than that of LiBaP. The LiSrP compound can be used as an absorptive layer in the energy range from 1.37 to 12 eV, whereas LiBaP can be used in the energy range from 0.84 to 9 eV.

The frequency-dependent reflectivity $R(\omega)$ spectra of the considered systems for both polarizations of the incident radiation are depicted in Fig. 6(b). The zero frequency limit R(0) is equal to 24 % (30 %) for $\vec{E}//a$ and 28 % (32 %) for $\vec{E}//c$ in LiSrP (LiBaP). The reflectivity $R(\omega)$ increases from R(0) with increasing photon energy to attain a maximum, and then a rapid decrease of $R(\omega)$ occurs at approximately 13.85 eV (5.88 eV) for $\vec{E}//a$ and 13.34 eV (5.41 eV) for $\vec{E}//c$. Fig. 6(b) shows that the maximum reflectivity in LiSrP (LiBaP) occurs at approximately 7.7 eV (1.62 eV) for $\vec{E}//a$ and at approximately 2.85 eV (2.44 eV) for $\vec{E}//c$. The maximum reflectivity is approximately 47 % (39 %) for $\vec{E}//a$ and 56 % (41 %) for $\vec{E}//c$ in LiSrP (LiBaP).

The energy-loss spectrum $L(\omega)$ describes the energy loss of a fast electron passing through a material [30]. The main peak in the $L(\omega)$ spectrum represents the characteristic associated with the plasma resonance; the corresponding frequency is called plasma frequency ω_P, which occurs when $\varepsilon_2(\omega) < 1$ and $\varepsilon_1(\omega)$ reaches a zero value [31]. From the energy-loss spectrum [Fig. 6(c)], the plasma frequency ω_p for LiSrP (LiBaP) is equal to approximately 13.85 eV (7.43 eV) for $\vec{E}//a$ and approximately 13.34 eV (6.05 eV) for $\vec{E}//c$. When the frequency of the incident

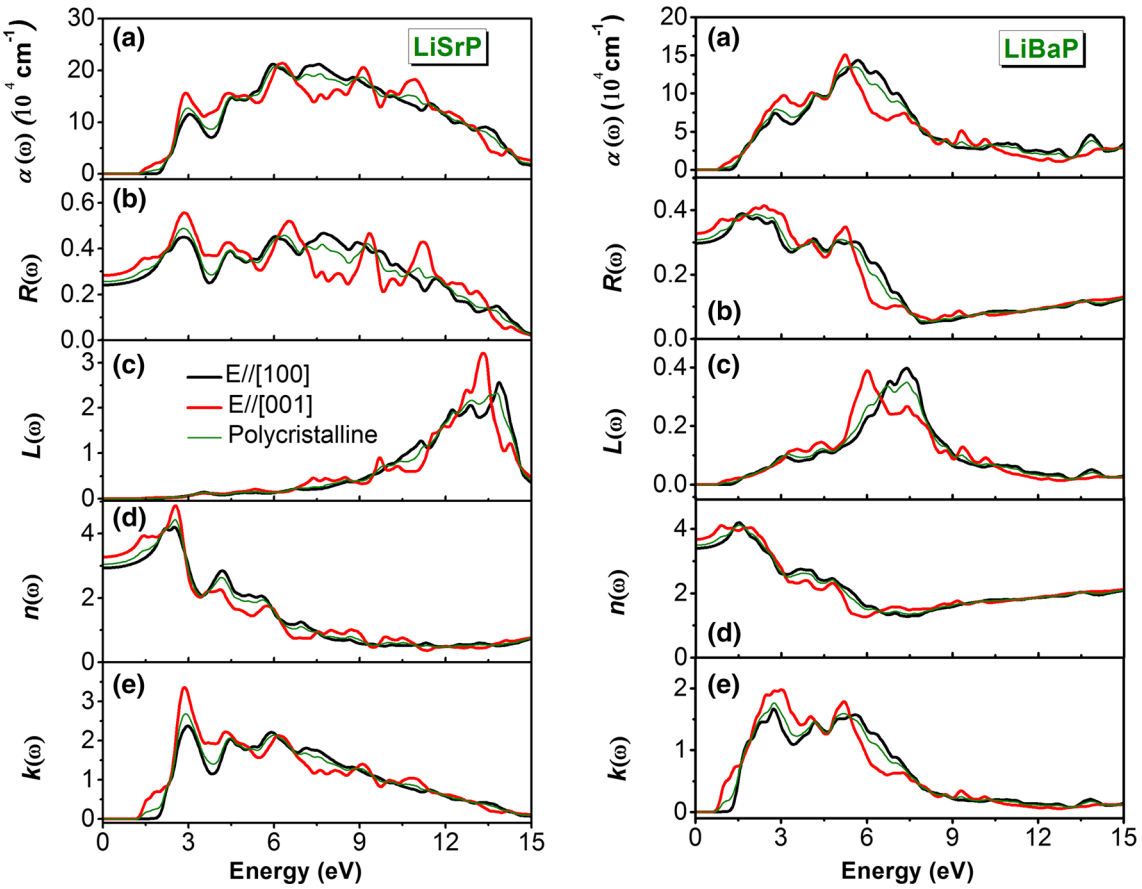

Fig. 6 Calculated optical function spectra: (**a**) absorption α(ω), (**b**) reflectivity R(ω), (**c**) energy loss function L(ω), (**d**) refractive index n(ω) and (**e**) extinction coefficient k(ω) for incident radiation polarized along the two principal crystallographic directions, i.e., $\vec{E}//a$ and $\vec{E}//c$, for the Li*Ae*P (*Ae* = Sr, Ba) crystals. Obtained spectra for the Li*Ae*P (*Ae* = Sr, Ba) polycrystals are also shown

light is higher than the plasma frequency, the material becomes transparent and hence an abrupt reduction of the reflectivity R(ω) occurs at the plasma frequency.

The refractive index $n(\omega)$ of a substance is the ratio of the speed of an electromagnetic wave in a vacuum to its speed in the substance. Knowledge of the refractive index of an optical material is important because its use in optical devices, such as photonic crystals and waveguides. The calculated refractive index spectra of LiSrP and LiBaP are shown in Fig. 6(d). The static refractive index $n(0)$ (the refractive index at zero energy) of LiSrP (LiBaP) is equal to 2.94 (3.39) for $\vec{E}//a$ and 3.27 (3.67) for $\vec{E}//c$. In both considered compounds, the refractive index increases with increasing energy, shows some peaks for the two polarization directions of the incident radiation and then decreases at high energy. Moreover, the refractive index for LiSrP goes below unity in certain energy ranges. When the refractive index is lower than unity, it indicates that the group velocity $V_g = c/n$ of the incident radiation is greater than the speed of light c, which means that the group velocity shifts to the negative domain and the nature of the medium changes from linear to non-linear. It is known that the refractive index has the same trend of variation with photon energy as the real part of the dielectric function, which means that all peaks appearing in the spectrum of the refractive index are related to the ones appearing in the real part of the dielectric function, whereas the extinction coefficient $k(\omega)$ [Fig. 6(e)] follows the imaginary part of the dielectric function. The polycrystalline sample optical behavior for both materials closely mimics the optical behavior observed for the [100] polarized incident light.

3.4. Thermodynamic properties

We have investigated the thermodynamic properties of the Li*Ae*P (*Ae* = Sr, Ba) systems in the temperature range from 0 to 800 K and the pressure range from 0 to 15 GPa using the quasi-harmonic Debye model as implemented in the Gibbs program [32]. A detailed description of the quasi-harmonic Debye model can be found elsewhere [32–36]. The relationship between the normalized unit-cell volume and temperature at some fixed pressures for LiSrP and LiBaP is shown in Fig. 7(a), which shows that the normalized volume V/V_0 is nearly constant at low

temperature and that an abrupt change occurs with increasing temperature. The normalized volume increases more rapidly at a high temperature for both compounds; however, the rate becomes a little slower with increasing pressure; these materials become less expandable at 15 GPa than at 0 GPa. The variation of the bulk modulus versus temperature at four fixed pressures (0, 5, 10 and 15 GPa) is depicted in Fig. 7(b). It can be seen that the bulk modulus remains nearly constant at a low temperature for both compounds and then decreases rapidly with increasing temperature; the increasing temperature causes a decrease in the hardness of materials due to the increase of the unit-cell volume. The bulk modulus values of LiSrP (LiBaP) at 0, 5, 10 and 15 GPa decrease by 29.43 % (32.70 %), 16.37 % (17.19 %), 10.75 % (10.86 %) and 7.92 % (7.62 %), respectively, when the temperature increases from 0 to 800 K. At zero pressure and temperature, our calculated bulk moduli for LiSrP and LiBaP are 45.12 GPa and 41.09 GPa, respectively. LiSrP is slightly more resistant to the compression of volume.

Figure 8(a) illustrates the variation in the Debye temperature θ_D as a function of temperature at some fixed pressures for LiSrP and LiBaP. It can be seen that θ_D decreases slightly with increasing temperature in both considered compounds. When the temperature increases from 0 to 800 K, the Debye temperature θ_D is reduced by 12.04 % (13.82 %) at 0 GPa, 6.11 % (6.24 %) at 5 GPa, 3.85 % (3.80 %) at 10 GPa and 2.82 % (2.65 %) at 15 GPa in LiSrP (LiBaP). This indicates that the reduction rate of θ_D with temperature becomes small at higher pressure; the high pressure suppresses the temperature effect on the Debye temperature. The calculated Debye temperatures θ_D at zero pressure and zero temperature are 398.27 K for LiSrP and 320.47 K for LiBaP.

The Grüneisen parameter describes the change in the vibrational properties of a crystal lattice due to the increase or decrease of its volume as a result of temperature change. The variation of the Grüneisen parameter as a function of temperature is shown in Fig. 8(b). At a given pressure, the Grüneisen parameter γ increases slowly with temperature. Moreover, the Grüneisen parameter γ increases more slowly at high pressure than at low pressure. At 300 K and zero pressure, our calculations yield a γ equal to 1.94 (2.073) for LiSrP (LiBaP).

Figures 9(a) and 9(b) show the temperature dependencies of the constant pressure heat capacity C_P and constant volume heat capacity C_V, respectively, at some fixed pressures. One can see that the constant volume heat capacity C_V and the constant pressure capacity C_P are very similar for the temperature range from 0 to approximately 300 K; C_V and C_P increase rapidly with temperature at a fixed pressure. When the temperature is higher than 300 K, the anharmonic effect on the heat capacity C_V is suppressed and increases slowly with increasing temperature to approach a constant value—the so-called Dulong–Pettit limit [37] which is common for all solids at high temperatures—whereas C_P still increases monotonously with increasing temperature. At high temperature, C_V approaches approximately 147.71 J mol^{-1} K^{-1} (148.77 J mol^{-1} K^{-1}) in LiSrP (LiBaP). At zero pressure and ambient temperature, C_V and C_P of LiSrP (LiBaP) are 137.88 J mol^{-1} K^{-1} (141.94 J mol^{-1} K^{-1}) and 144.37 J mol^{-1} K^{-1} (149.47 J mol^{-1} K^{-1}), respectively.

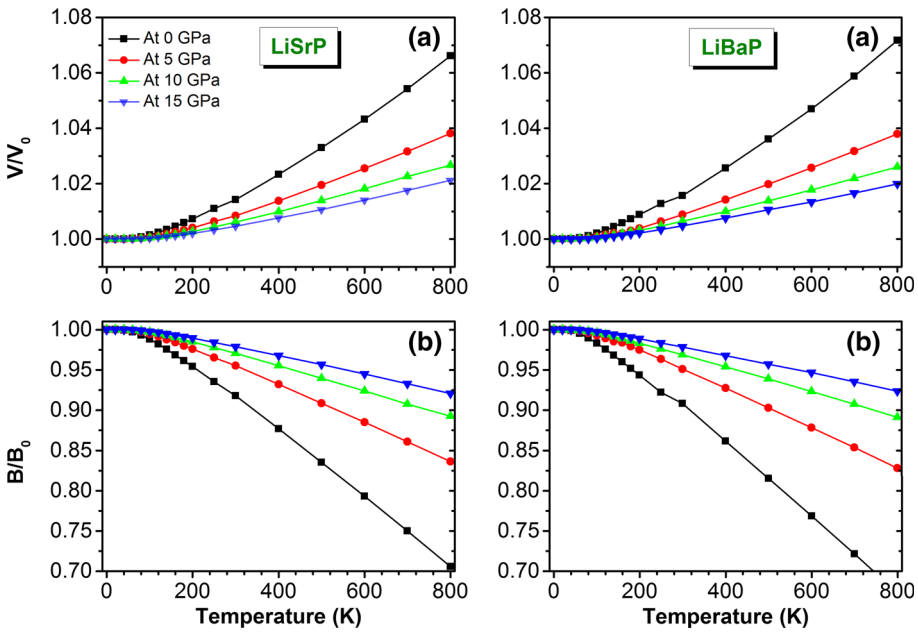

Fig. 7 (**a**) The normalized primitive-cell volume V/V_0 as a function of temperature for the LiSrP and LiBaP compounds at some fixed pressures; V is the primitive-cell volume at the considered temperature; V_0 is the primitive-cell volume at zero temperature. (**b**) The normalized bulk modulus B/B_0 as a function of temperature for the LiSrP and LiBaP compounds at some fixed pressures; B is the bulk modulus at the considered temperature and B_0 is the bulk modulus at the zero temperature

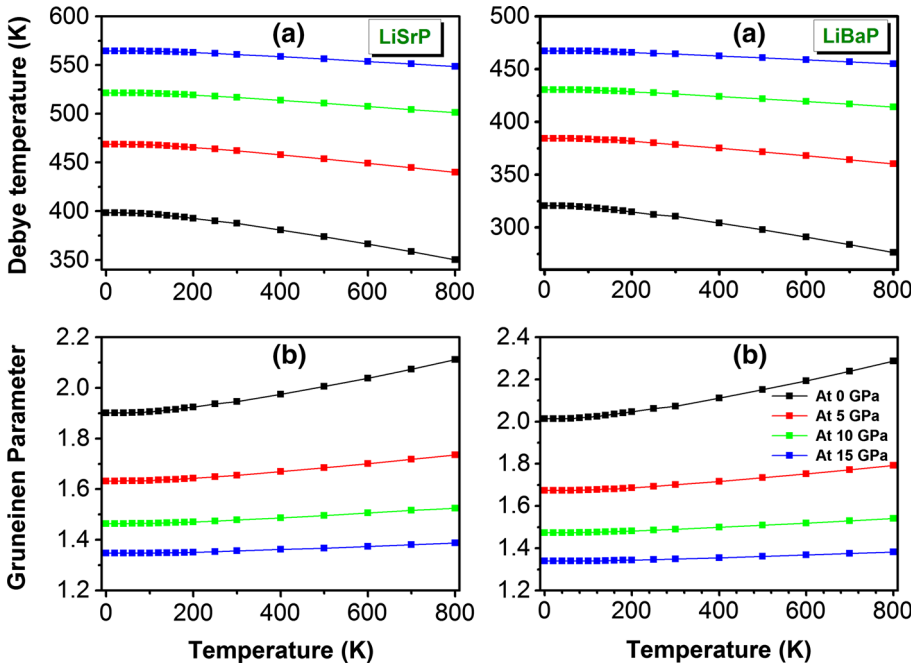

Fig. 8 (**a**) Variations of the Debye temperature and (**b**) Grüneisen parameter versus temperature at some fixed pressures for the LiSrP and LiBaP compounds

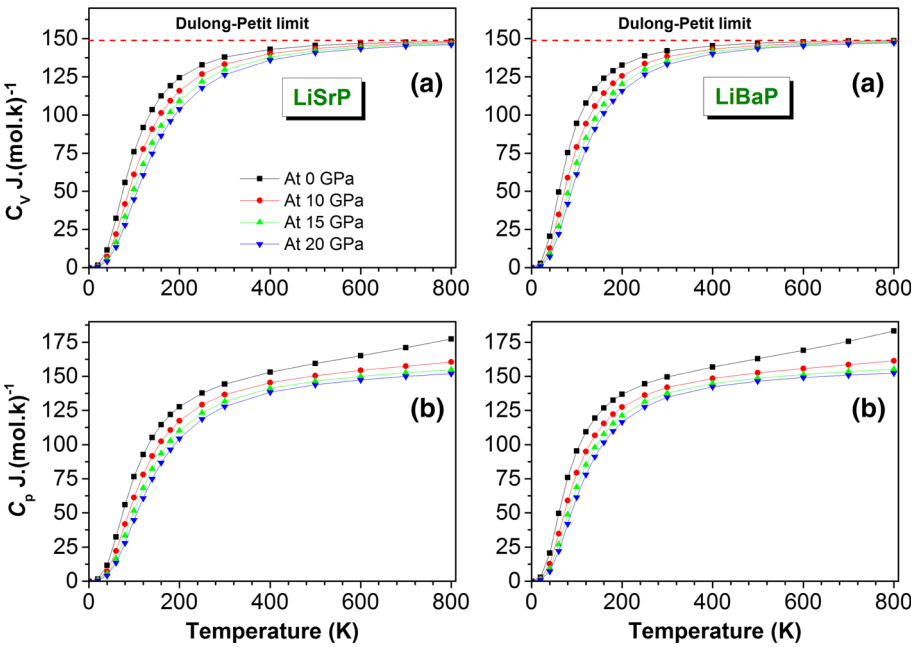

Fig. 9 (**a**) Variations of the heat capacity at constant volume C_V and (**b**) the heat capacity at constant pressure C_P versus temperature at some fixed pressures for the LiSrP and LiBaP compounds

Variations in the volume thermal expansion coefficient α of LiSrP and LiBaP as a function of temperature T at certain fixed pressures are shown in Fig. 10. For $T \leq 250$ K, the thermal expansion coefficient α increases rapidly with increasing temperature at fixed pressure in both considered compounds. For $T > 250$ K, the increase of α with increasing temperature becomes more gradual and approaches a linear behavior. The rate of increase of α with increasing temperature decreases with increasing pressure. Figure 10 shows that the pressure effect on α is small at low temperature and becomes substantial at high temperature. This means that there is a large volume thermal expansion coefficient at low pressure, which is in accordance with the variation of the unit-cell volume with pressure and temperature. At zero pressure and room temperature, α is approximately equal to 8.0672 K^{-1} for LiSrP and 8.5318 K^{-1} for LiBaP.

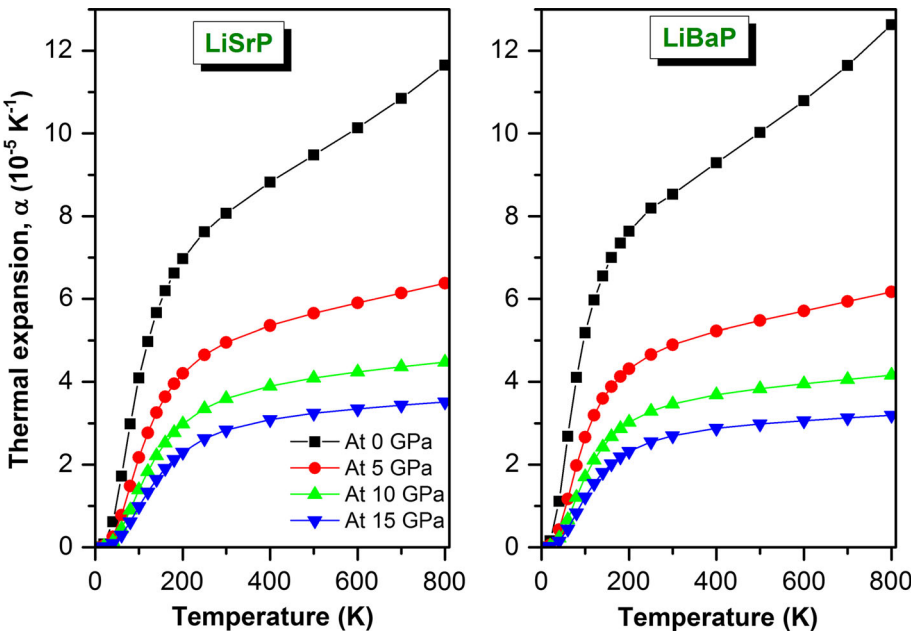

Fig. 10 Variation of the volume thermal expansion coefficient as a function of temperature at some fixed pressures for LiSrP and LiBaP

4. Conclusions

Ab initio calculations based on the DFT within the GGA-PBEsol are performed to investigate the systematic trends for the structural, electronic, optical and thermodynamic properties of the Li*Ae*P family, depending on the type of the alkaline earth (*Ae*) elements (*Ae* are Sr and Ba). First, the optimized structural parameters are obtained and compared with the available data in the scientific literature. The good agreement between our calculated structural parameters and their corresponding measured ones confirms the reliability of the used calculation approaches. The examined materials have an indirect band gap. The value of the fundamental energy gap decreases when the *Ae* atom in the isostructural Li*Ae*P series is substituted in the sequence: *Sr* → *Ba*. Analysis of the bonding properties via the density of states and charge density maps reveals that the considered materials are rather covalent. Optical functions are predicted for two different polarizations of the incident radiations for an energy range up to 20 eV. The obtained optical spectra exhibit a strong optical anisotropy. LiSrP is more absorptive than LiBaP. The static dielectric function of LiBaP is larger than that of LiSrP, which can be explained on the basis of the Penn model. The obtained results through the quasi-harmonic Debye model show that at a fixed pressure the increase of temperature leads to an increase in the unit-cell volume, heat capacity and volume thermal expansion coefficient, but it leads to a decrease in the bulk modulus and Debye temperature. At a fixed temperature, the increase of pressure leads to the increase of the bulk modulus and Debye temperature whereas it leads to the decrease of the unit-cell volume, volume thermal expansion coefficient and heat capacity. There are no available experimental data for the electronic, optical and thermodynamic properties of the examined materials; our results are therefore purely theoretical predictions and must be tested experimentally in the future.

Acknowledgments The authors extend their appreciation to the International Scientific Partnership Program ISPP at King Saud University for funding this research work through JSPP# 0025.

References

[1] M L Fornasini and F Merlo *J. Alloys Compd.* **219** 63 (1995)
[2] T Graf, C Felser and S S P Parkin *Prog. Solid State Chem.* **39** 1 (2011)
[3] F Casper, R Seshadri and C Felser *Phys. Status Solidi A* **206** 1090 (2009)
[4] B Balke, J Barth, M Schwall, G H Fecher and C Felser *J. Electron. Mater.* **40** 702 (2011)
[5] S Chadov, X Qi, J Kübler, G H Fecher, C Felser and S C Zhang *Nature Mater.* **9** 541 (2010)
[6] H Lin, L A Wray, Y Xia, S Xu, S Jia, R J Cava, A Bansil and M Z Hasan *Nature Mater.* **9** 546 (2010)
[7] J W Bennett, K F Garrity, K M Rabe and D Vanderbilt *Phys. Rev. Lett.* **109** 167602 (2012)
[8] Q D Gibson, L M Schoop, L Müchler, L S Xie, M Hirschberger, N P Ong, C Car and R J Cava *arXiv preprint arXiv*: 1411.0005, 2014
[9] X Wan, A M Turner, A Viswanathan and S Y Savrasov *Phys. Rev. B* **83** 205101 (2011)
[10] A A Burkov and L Balents *Phys. Rev. Lett.* **107** 127205 (2011)
[11] S M Young, S Zaheer, J C Y Teo, C L Kane, E J Mele and A M Rappe *Phys. Rev. Lett.* **108** 140405
[12] Z Wang, Y Sun, X Q Chen, C Franchini, G Xu, H Weng, X Dai and Z Fang *Phys. Rev. B* **85** 195320 (2012)
[13] Z K Liu *et al. Science* **343** 864 (2014)

[14] Z Wang, H Weng, Q Wu, X Dai and Z Fang *Phys. Rev. B* **88** 125427 (2013)
[15] M Reffas, A Bouhemadou, R Khenata, T Ouahrani and S Bin-Omran, *Phys. B Condensed Matter* **405** 4079 (2010)
[16] Y Dong and F J DiSalvo *J Solid State Chem.* **180** 432 (2007)
[17] G Brauer and E Zintl *Z Phys Chem* B **37** 323 (1937)
[18] S J Clark, M D Segall, C J Pickard, P J Hasnip, M J Probert, K Refson and M C Payne *Zeitschrift fuer Kristallographie* **220** 567 (2005)
[19] J P Perdew *et al*. *Phys. Rev. Lett.* **10** 136406 (2008)
[20] D Vanderbilt *Phys. Rev. B* **41** 7892 (1990)
[21] H J Monkhorst and J D Pack *Phys. Rev. B* **13** 5188 (1976)
[22] T H Fischer and J Almlof *J. Phys. Chem.* **96** 9768 (1992)
[23] S Zh Karazhanov, P Ravindran, H Fjellvag and B G Svensson *J. Appl. Phys.* **106** 123701 (2009)
[24] P W Tasker *J. Phys. C: Solid State Phys.* **12** 4977 (1979)
[25] L Makinistian and E A Albanesi *Phys. Rev. B* **74** 045206 (2006)
[26] M Alouani and J M Wills *Phys. Rev. B* **54** 2487 (1996)
[27] M Fox *Optical Properties of Solids* (New York: Oxford University Press) (2001)
[28] M Dressel and G Gruner *Electrodynamics of Solids: Optical Properties of Electrons in Matter* (United Kingdom: Cambridge University Press) (2002)
[29] D R Penn *Phys. Rev.* **128** 2093 (1962)
[30] A Bouhemadou and R Khenata *Comput. Mater. Sci.* **39** 803 (2007)
[31] R Saniz, L H Ye, T Shishidou and A J Freeman *Phys. Rev. B* **74** 014209 (2006)
[32] M A Blanco, E Francisco and V Luaña *Comput. Phys. Commun.* **158** 57 (2004)
[33] A Bouhemadou, R Khenata and B Amrani *Physica B: Condensed Matter* **404** 3534 (2009)
[34] M Flórez, J M Recio, E Francisco, M A Blanco and A M Pendás *Phys. Rev. B* **66** 144112 (2002)
[35] E Francisco, J M Recio, M A Blanco and A M Pendás *J. Phys. Chem. A* **102** 1595 (1998)
[36] E Francisco, M A Blanco and G Sanjurjo *Phys. Rev. B* **63** 049107 (2001)
[37] A T Petit and P L Dulong *Ann. Chim. Phys.* **10** 395 (1819)